Chapter 4

Statistics of SAR Images

The purpose of this chapter is to examine the statistics of SAR images that can have an influence on the development of detectors. Because of the properties of the speckle in SAR images, detectors (e.g. edge detectors) that work well in visual or infrared images fail in SAR images. However, because for the major part of the images, the statistics of the speckle are well known and can be modeled accurately, this information can be used in the development of a detector. The first part of this chapter presents an overview of the statistics of speckle in uniform regions. Another important aspect is the relationship between different components of multi-dimensional SAR images. This is investigated in the second part of the chapter. In all parts the theoretical results are checked with information extracted from a polarimetric SAR image.

4.1 Statistics of the Speckle in SAR Images

The primary geophysical quantity determining the appearance of the SAR data is the complex radar reflectivity. This radar reflectivity expresses the fact that, when an electromagnetic wave scatters from a given position of the earth surface, the physical properties of the terrain cause changes in both the phase $\Phi(x, y)$ and amplitude $A(x, y)$ of the wave. The SAR basically measures the amplitude and phase of the returned signal which can be expressed as a complex number:

$$C = Ae^{i\Phi} = Re(C) + i * Im(C). \tag{4.1}$$

In this form the SAR image is known as the *(Single-Look) Complex image (SLC)*. Usually the image format provides the "real" and "imaginary" component of the signal.

From this image a variety of other images can be formed such as the *amplitude image*, the *phase image* and the *intensity image* ($I = A^2$). Often, the *Log-Intensity image* is also used. The image of $10log_{10}I$ is a linearly scaled estimate of the radar backscattering coefficient σ_0 in dB [10] and furthermore, as we will see, its variance in uniform regions is independent of σ_0.

All of these images appear quite different. However, they all have in common that even for surfaces of uniform terrain properties, they appear noisy. The noise-like characteristic of these images that can be found in any image produced by a coherent imaging system (e.g. laser, sonar, ultrasound) is called *Speckle*. In this section the statistical properties

of this speckle in uniform regions will be examined. Some understanding of the statistics of the speckle in the different images is important for developing detectors and deciding which type of image (i.e. complex, amplitude, intensity or Log-Int) is most suited for this detection.

The theoretical probability distributions of speckle in the different images that are given in literature are verified with our data in the following way. On the original Single-Look Complex (SLC) image a uniform region of 100×100 pixels, was delimited. Then the original complex image was transformed into the different other image types. For each of them the histogram of the values inside the test area were determined. The theoretically expected distribution was fitted to these data and the quality of the fit was verified visually as well as by means of a χ^2 test.

4.1.1 The Origin of Speckle

In distributed targets each resolution cell of the imaging system contains a large number N of discrete scatterers. As the wave interacts with the target, each individual scatterer contributes a backscattered wave with a phase and amplitude change, so the total returned wave is:

$$\vec{E} = Ae^{i\Phi} = \sum_{i=1}^{N} \frac{1}{\sqrt{N}} a_k e^{i\Phi_k}. \tag{4.2}$$

The resolution in range is typically several times the wavelength of the radiation emitted by the radar. Hence, even if all elementary scatterers were identical, the waves scattered from them have very different path lengths. The individual scatterers therefore produce a very different phase in the incident wave. In fact the phase is uniformly distributed in $[-\pi, \pi]$.

The sum in 4.2 can now be seen as a random walk in the complex plane where each step a_k is in a completely different direction. This problem is thoroughly treated in many books about SAR (e.g. [10, 11]) as well as in [12] which treats about laser speckle. The hypotheses made by Goodman [12] are:

- the amplitude a_k and the phase Φ_k produced by the k^{th} individual scatterer are statistically independent of each other and of the amplitudes and phases of all other elementary scatterers
- the phases Φ_k are uniformly distributed in $[-\pi, \pi]$

The result for the different types of SAR images is given in the next paragraphs.

4.1.2 The Real and Imaginary Part of the SLC

Goodman [12] shows that the assumptions mentioned at the end of the previous paragraph have the following consequences for the real and imaginary component of the resultant field:

- the average over an ensemble containing many scatterers is zero:

$$< Re(E) >=< Im(E) >= 0, \tag{4.3}$$

- the variance for the real and imaginary component are both equal to:

$$< [Re(E)]^2 >=< [Im(E)]^2 >= \frac{1}{N}\sum_{k=1}^{N}\frac{<\mid a_k \mid^2>}{2}, \tag{4.4}$$

- the correlation between real and imaginary components is zero:

$$< [Re(E)Im(E)] >= 0. \tag{4.5}$$

Thus the real and imaginary components of the complex (electric) field have zero means, identical variances and they are uncorrelated. Furthermore, if each resolution cell contains many individual scatterers, the central limit theorem implies that the real and imaginary components of the complex field are asymptotically Gaussian. The consequence is that the joint probability density function of the speckle in a uniform region of the complex image is a special case of a bi-variate normal distribution with zero mean, zero correlation and identical variances. This results in [10, 11, 12]:

$$P_{(Re(E),Im(E))}(Re(E), Im(E)) = \frac{1}{2\pi\sigma^2} exp\left(-\frac{(Re(E))^2 + (Im(E))^2}{2\sigma^2}\right). \tag{4.6}$$

This is also called circular Gaussian density function since contours of constant density are circles in the complex plane.

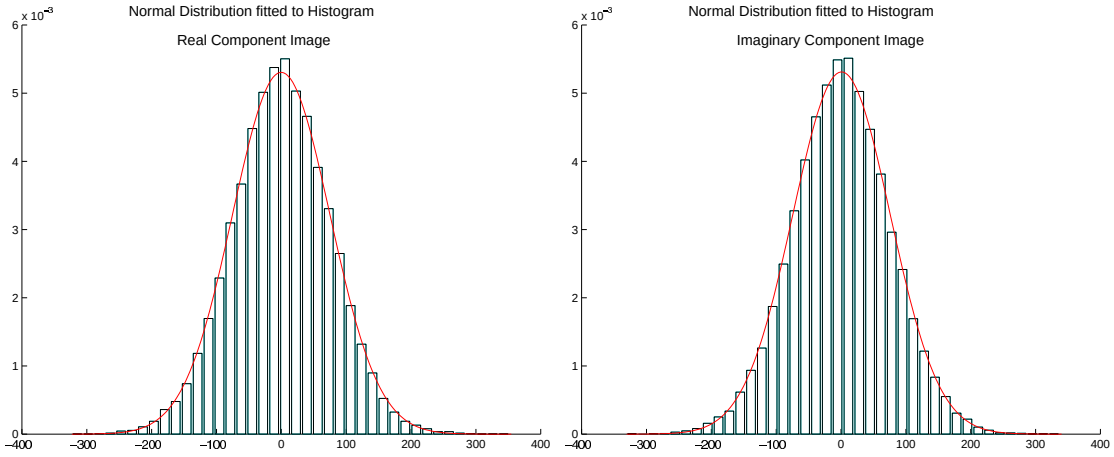

Figure 4.1: Speckle distribution in a uniform region of the real (left) and imaginary (right) component of the SLC image

To have a feeling of how well the data actually correspond to the model for the different images, we estimated the model's parameters from a uniform region. We used the same region in all images and each time give the 95% confidence interval (CI) as well as the results of the χ^2-test (the p-values [1] are given).

[1] p-value: probability of the test statistic being as extreme as the one observed given that the null-hypothesis is true

For the Real Component:	μ	= -0.175	$CI : [-1.157, 0.806]$
	σ	= 75.193	$CI : [74.505, 75.893]$
	p-value of χ^2 test	= 0.39	
For the Imaginary Component:	μ	= 0.802	$CI : [-0.178, 1.783]$
	σ	= 75.108	$CI : [74.421, 75.808]$
	p-value of χ^2 test	= 0.38	

The confidence intervals show that the mean values are indeed zero and the standard deviations are equal. The p-value of the χ^2 test shows a very good correspondence between the histogram of the measured values and the theoretical normal distribution.

4.1.3 The Amplitude Image

The amplitude $A = \sqrt{ReE^2 + ImE^2}$ is Rayleigh distributed:

$$P_A(A) = \frac{A}{\sigma^2} exp\left(-\frac{A^2}{2\sigma^2}\right) \tag{4.7}$$

and the mean is $\mu_A = \sqrt{\frac{\pi}{2}}\sigma$, the standard deviation is $\sigma_A = \sigma\sqrt{2 - \frac{\pi}{2}}$.

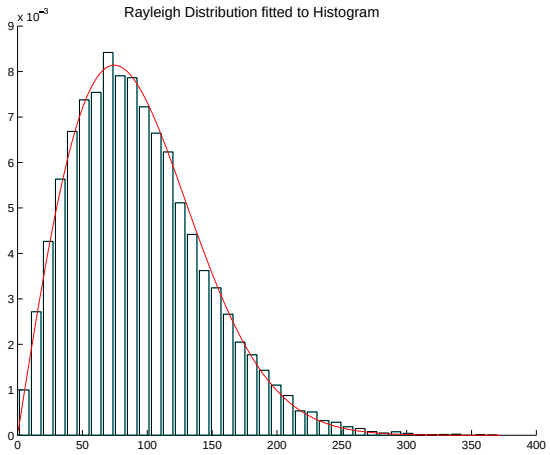

Figure 4.2: Speckle distribution in a uniform region of the amplitude image

$\sigma = \mu_A\sqrt{\frac{2}{\pi}}$	= 74.498
p-value of χ^2 test	= 0.97

4.1.4 The Intensity Image

The intensity, defined as $I = A^2$ follows a negative exponential law given by:

$$P_I(I) = \frac{1}{2\sigma^2} exp\left(-\frac{I}{2\sigma^2}\right). \tag{4.8}$$

Its mean is equal to its standard deviation: $\mu_I = \sigma_I = 2\sigma^2$. For that reason speckle is sometimes called "multiplicative noise" with a signal-to-noise ratio equal to $SNR = \mu_I/\sigma_I = 1$.

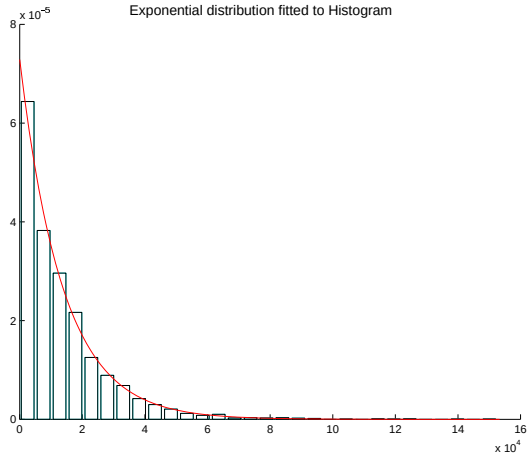

Figure 4.3: Speckle distribution in a uniform region of the intensity image

$2\sigma^2 \quad = 11295.345 \quad CI : [11148, 11443]$
p-value of χ^2 test $= 0.52$

4.1.5 The Log-Intensity Image

The Log-Intensity is defined as $D = log(I)$ in which "log" is the natural (base e) logarithm. D follows a Fisher-Tippet distribution given by:

$$P_D(D) = \frac{e^D}{2\sigma^2} e^{-\frac{e^D}{2\sigma^2}}. \tag{4.9}$$

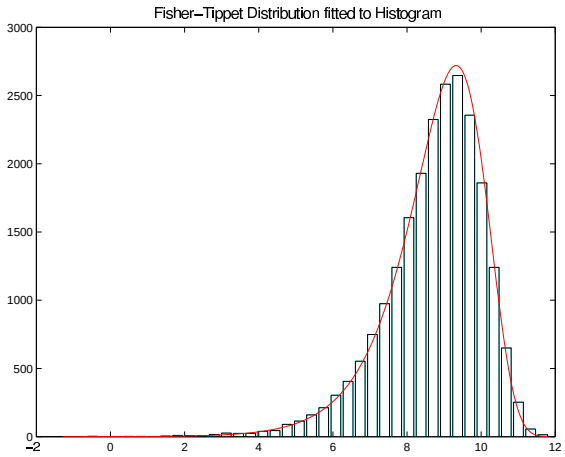

Figure 4.4: Speckle distribution in a uniform region of the log-intensity image

Its mean is equal to $\mu_D = log(2\sigma^2) - \gamma_e$ where γ_e is Euler's constant (=0.577). The variance is a constant equal to $\sigma_D^2 = \frac{\pi^2}{6}$. The variance thus does not depend on the radar reflectivity in the region.

$\mu_D = 8.7164$
$\sigma_D = 1.3233$

4.1.6 Remarks

The basic assumption underlying the distributions found above, was that the individual scatterers in uniform regions are much smaller than the spatial resolution of the SAR. This was almost always true for low-resolution SAR systems. However, especially the new generation airborne SAR systems, have a high resolution (1 m or less). For some types of regions such as forests and sea surface under windy conditions, this assumption is not valid and other distributions are more appropriate (e.g. the log-normal, Weibull, K- or gamma distribution). For fields the distributions discussed above apply, for forests a K-distribution is more appropriate [10]. Obviously for highly textured regions (e.g. built-up areas), which even on low-resolution SAR do not appear uniform, the distributions given are not valid either.

4.2 Second Order Statistics

In this section we will examine the relation between neighbouring pixels in the same image as well as between different images. Of particular interest is the spatial correlation function in one image along the range and azimuth direction. We will see in chapter 5 that the spatial correlation influences the behaviour of edge detectors. The relation between the real and imaginary part of the SLC image and between the different polarisation images will also be examined. The latter, i.e. the relation (or correlation) between the different polarisation images, will be used in chapter 7 for detecting built-up areas.

4.2.1 Spatial Correlation

If the pixel spacing in an image is smaller than the resolution of the sensor, a correlation exists between neighbouring pixels. Optical sensors often have the same pixel spacing in both X and Y direction and have a circular symmetrical point spread function (same resolution in X- and Y- direction). Therefore their autocorrelation function is usually circular symmetrical. For SAR, the specific processing in range and azimuth causes differences in resolution between both directions and thus the amount of correlation is usually different in range and azimuth direction. To estimate this effect, the spatial correlation coefficient was measured, for different displacements, in different uniform regions. Because we will mainly use the SLC and the log-intensity images in the development of the different detectors proposed in this thesis, the spatial correlation function will be investigated in these types of images. For the SLC image the real component image is used.

The spatial correlation coefficient is defined as:

$$\rho(\Delta x, \Delta y) = \frac{\langle (I(x+\Delta x, y+\Delta y) - \mu_I)(I(x,y) - \mu_I) \rangle}{\sigma_I^2}, \tag{4.10}$$

where μ_I and σ_I are respectively the average and standard deviation of the image values inside the homogeneous region and $\langle . \rangle$ denotes the average over the surface of the region. ρ was calculated for various values of Δ_x and Δ_y.

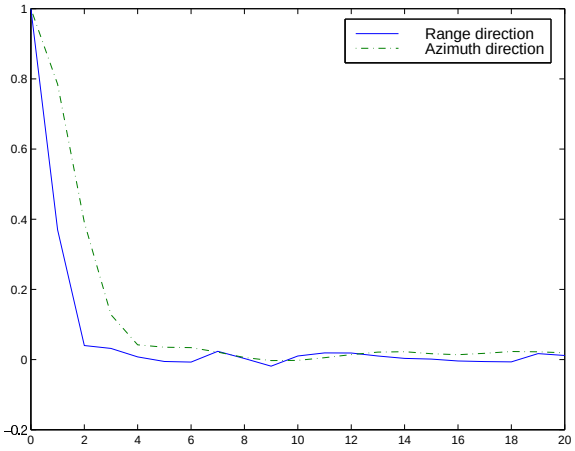

Figure 4.5: Spatial correlation vs.translation distance in range and azimuth direction for a uniform region (field)

Fig 4.5 shows the spatial correlation function in range and azimuth direction. From fig 4.5 it appears that the correlation length in the azimuth direction (3) is slightly longer than the one in the range direction (2). This can be partly explained by the fact that the ratio of spatial resolution to pixel spacing is larger in azimuth than in range direction (see table 4.1). The values in the table are measured on the test image (L-Band E-SAR image), they are thus specific properties of sampling in the L-Band E-SAR system. However, the fact that the spatial correlation is larger in azimuth direction than in range direction in single-look images is true for most SAR systems.

Image direction	Resolution	Pixel Spacing
Range direction	1.49854	1.49854
Azimuth direction	1.20000	0.467145

Table 4.1: Resolution and pixel spacing for the E-SAR images

Please note that the correlation function is sensitive to underlying texture (that is not due to speckle). To illustrate this, we identified 6 regions with different land cover and calculated the correlation function in the range and azimuth direction. The results are shown in fig. 4.6. The first sample of type "city" contains blocks of buildings, aligned in azimuth direction. Obviously this results in a very high correlation along this direction.

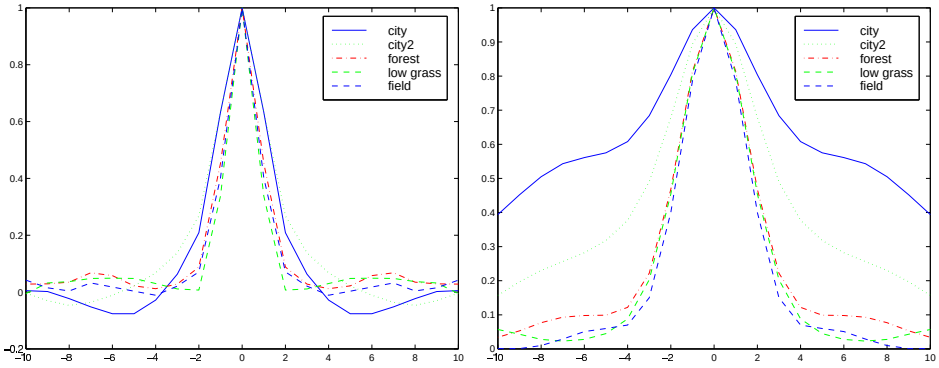

Figure 4.6: Spatial correlation function for various types of land covers in range (left) and azimuth (right)

In fig. 4.7 the selected regions for each of the landcovers are shown. As the purpose is to provide a visual appreciation of the spatial correlation within these regions, each was rescaled between greyvalues 0 and 255. The values are thus not comparable between images.

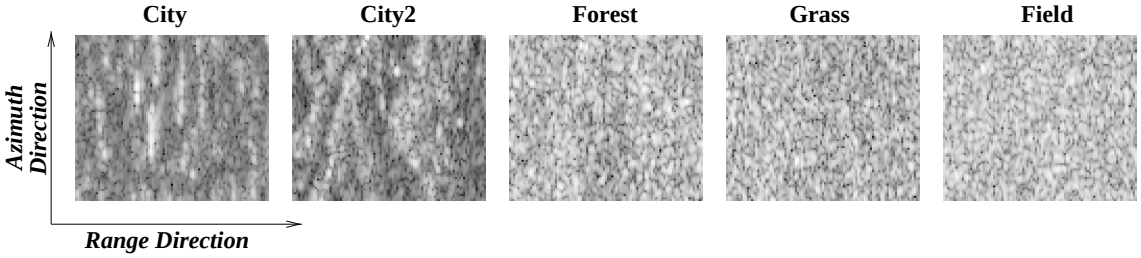

Figure 4.7: Selected image regions of different landcovers.

In order to obtain an estimation of the correlation function in uniform regions, we identified 15 uniform regions and calculated the average correlation function. Figure 4.8 shows the uniform regions that were selected. Most of them correspond to fields with varying brightness and two regions (nrs 4 and 13) are in the forest. Please note that all selected regions have a dimension of 100×100 pixels in the original slant range image and that the image has been turned 90 degrees for printing, i.e. the azimuth direction is horizontal in the figure and this direction has been reduced, again for display reasons.

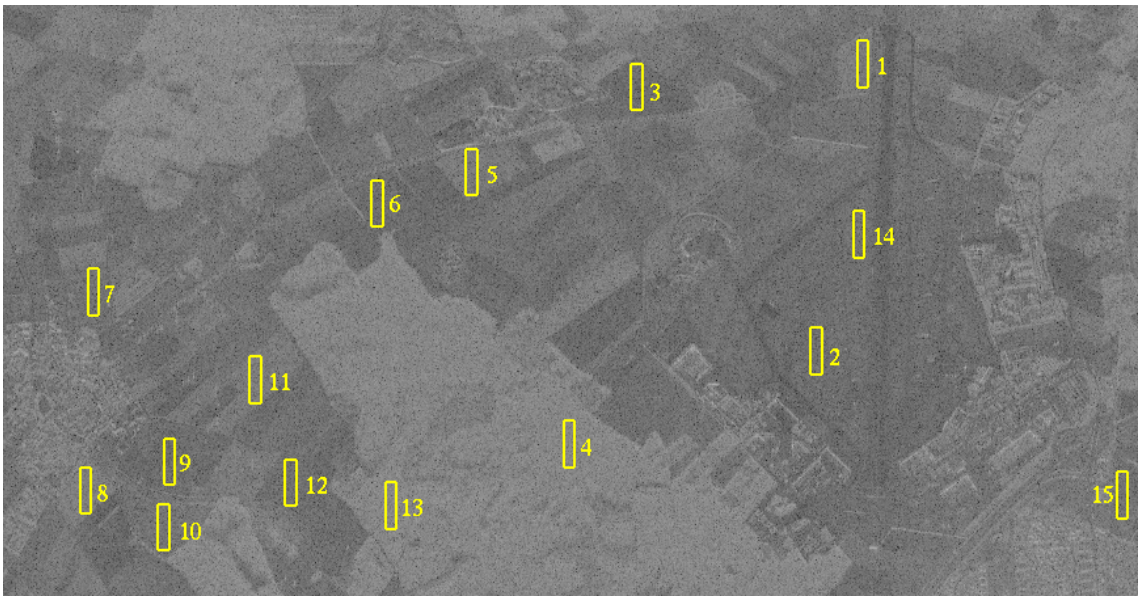

Figure 4.8: Overview of the selected uniform regions

The spatial correlation in a SAR image is caused by the combined effect of the SAR system (its impulse response) and a terrain component (caused by texture). In all non-textured regions the spatial correlation function should be the same. For the SLC image it is given by [23, 10]:

$$\rho_S(\Delta_x, \Delta_y) = \frac{\int_{-\infty}^{+\infty}\int_{-\infty}^{+\infty} h^*(x,y)h(x-\Delta_x, y-\Delta_y)dxdy}{\int_{-\infty}^{+\infty}\int_{-\infty}^{+\infty} \mid h(x,y) \mid^2 dxdy}, \tag{4.11}$$

with h the impulse response of the SAR system.

In order to verify that the 15 selected uniform regions are non-textured, we have determined their average correlation function and then compared the correlation function for each of the 15 regions with this average. The results are shown in figs. 4.9 and 4.10. The solid lines correspond to the average correlation function, the dashed line is the correlation function for the considered "uniform" region. Visual inspection of the two figures shows that several of the "uniform regions" have a correlation function that differs from the average.

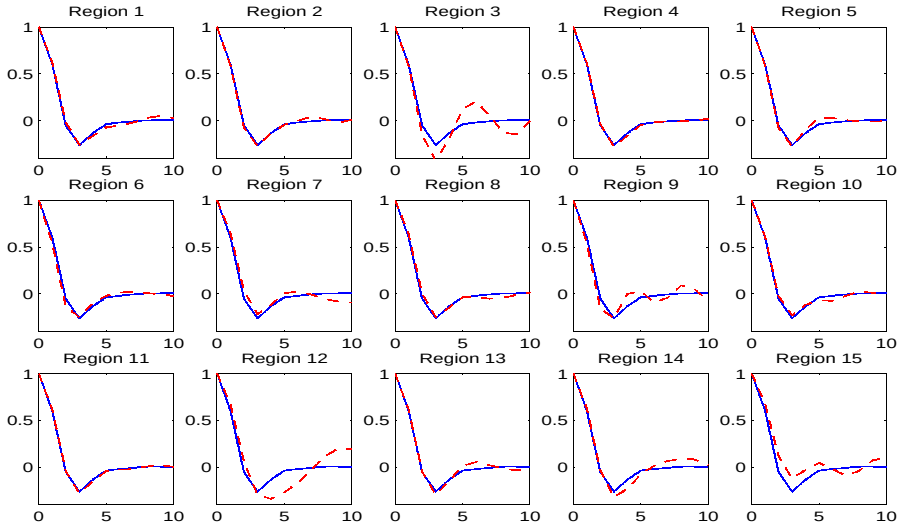

Figure 4.9: Autocorrelation function in the range direction for the 15 uniform regions

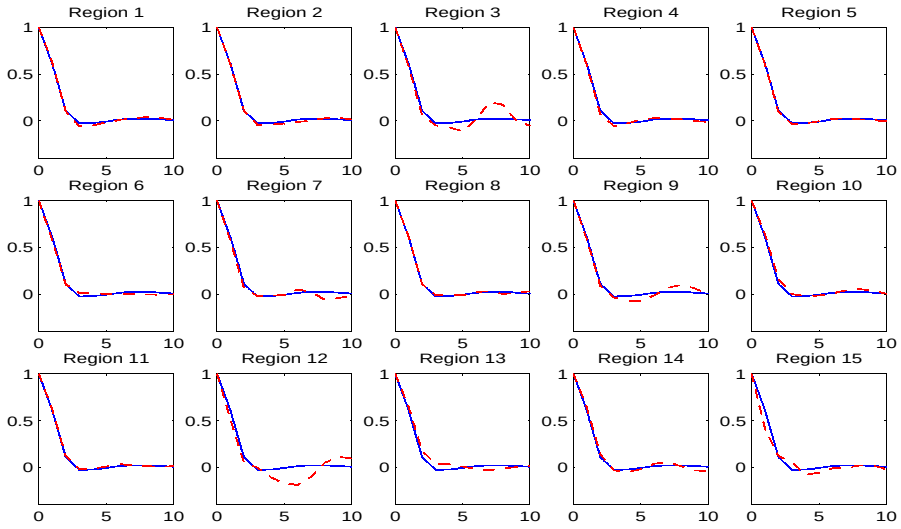

Figure 4.10: Autocorrelation function in the azimuth direction for the 15 uniform regions

Figure 4.11 shows the average spatial correlation functions in range and azimuth direction for the three polarisations in the real component image and in fig. 4.12 the same is shown for the Log-Intensity image. The average correlation function does not depend on the polarisation for uniform regions. The values of the average correlation function for the three polarisations are given in table 4.2 and 4.3.

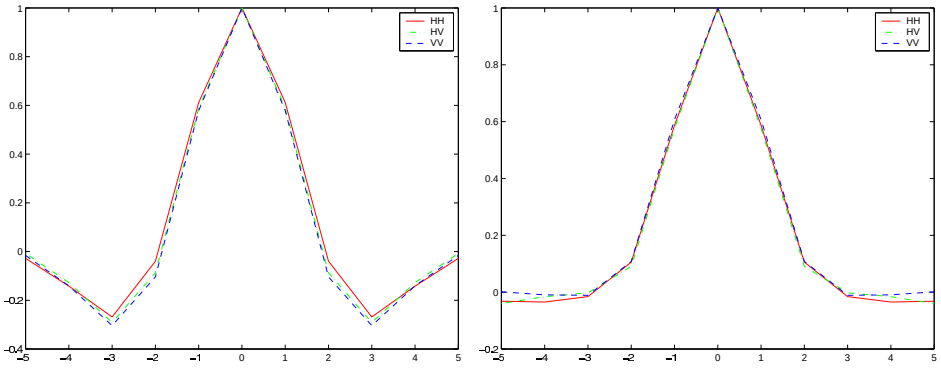

Figure 4.11: Average correlation function in range (left) and azimuth (right) direction in the real component image

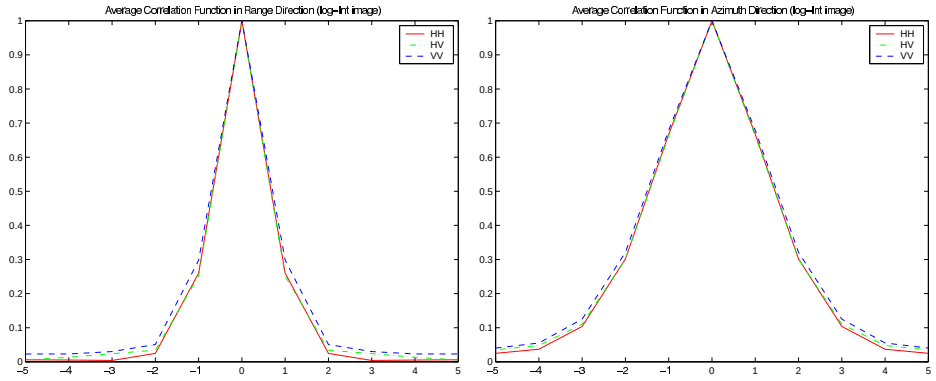

Figure 4.12: Average correlation function in range (left) and azimuth (right) direction in the log-intensity image

HH	Azimuth →					
Range	1.0000	0.6118	-0.0397	-0.2685	-0.1419	-0.0278
↓	0.5871	0.4240	0.0265	-0.1600	-0.1057	-0.0302
	0.1057	0.1187	0.0522	-0.0099	-0.0224	-0.0083
	-0.0156	0.0039	0.0220	0.0189	0.0084	0.0073
	-0.0348	-0.0119	0.0175	0.0203	0.0101	0.0066
	-0.0319	-0.0087	0.0224	0.0253	0.0127	0.0067
HV:	Azimuth →					
Range	1.0000	0.5884	-0.0869	-0.2914	-0.1272	-0.0075
↓	0.5765	0.3801	-0.0155	-0.1653	-0.0868	-0.0090
	0.0909	0.0847	0.0370	0.0026	-0.0087	-0.0057
	-0.0021	-0.0095	0.0037	0.0156	0.0155	0.0150
	-0.0159	-0.0070	0.0020	0.0011	0.0106	0.0293
	-0.0401	0.0055	0.0319	0.0181	0.0083	0.0172
VV:	Azimuth →					
Range	1.0000	0.5783	-0.1041	-0.3040	-0.1405	-0.0159
↓	0.6071	0.4394	0.0029	-0.1867	-0.1077	-0.0169
	0.1083	0.1183	0.0379	-0.0255	-0.0283	-0.0106
	-0.0111	0.0025	0.0133	0.0123	0.0045	-0.0033
	-0.0095	-0.0082	0.0001	0.0088	0.0103	0.0019
	0.0013	0.0019	0.0019	0.0037	0.0069	0.0047

Table 4.2: Values of the correlation function for the 3 polarisations in the real image

HH	Azimuth →					
Range	1.0000	0.6671	0.3019	0.1036	0.0369	0.0249
↓	0.2599	0.2237	0.1285	0.0543	0.0246	0.0205
	0.0247	0.0260	0.0187	0.0144	0.0173	0.0195
	0.0041	0.0023	0.0027	0.0071	0.0157	0.0201
	0.0051	0.0026	0.0049	0.0113	0.0165	0.0206
	0.0059	0.0034	0.0049	0.0075	0.0088	0.0073
HV:	Azimuth →					
Range	1.0000	0.6623	0.3013	0.1104	0.0479	0.0351
↓	0.2517	0.2069	0.1130	0.0469	0.0242	0.0196
	0.0340	0.0305	0.0233	0.0159	0.0131	0.0138
	0.0238	0.0210	0.0198	0.0177	0.0151	0.0129
	0.0133	0.0122	0.0088	0.0086	0.0121	0.0145
	0.0053	0.0107	0.0139	0.0139	0.0148	0.0145
VV:	Azimuth →					
Range	1.0000	0.6789	0.3208	0.1251	0.0551	0.0402
↓	0.2977	0.2567	0.1573	0.0817	0.0510	0.0453
	0.0507	0.0508	0.0475	0.0424	0.0416	0.0422
	0.0301	0.0319	0.0318	0.0301	0.0304	0.0317
	0.0231	0.0268	0.0288	0.0277	0.0258	0.0244
	0.0229	0.0240	0.0246	0.0255	0.0268	0.0261

Table 4.3: Values of the correlation function for the 3 polarisations in the log-int image

4.2.2 Relation between Real and Imaginary Components

The real and imaginary components of the SLC image in uniform regions are uncorrelated. The correlation coefficient measured in a homogeneous region was -0.002432. A scatterplot of values of the real and imaginary part results in a circular symmetrical structure caused by the bi-variate normal distribution mentioned in section 4.1.2 This de-correlation is valid in all regions with fully developed speckle (uniform regions). It is not valid at locations with a high number of deterministic scatterers in the image (e.g. in some parts of a village).

4.2.3 Interchannel Correlation

The interchannel correlation is the correlation between the different polarisations in our case, i.e. between HH, VV and HV. The interchannel correlations are defined as:

$$\rho_{HH/HV} = \frac{\mid \langle S_{HH} S_{HV}^{*} \rangle \mid}{\sqrt{\langle \mid S_{HH} \mid^{2} \rangle \langle \mid S_{HV} \mid^{2} \rangle}}, \tag{4.12}$$

$$\rho_{VV/HV} = \frac{\mid \langle S_{VV} S_{HV}^{*} \rangle \mid}{\sqrt{\langle \mid S_{VV} \mid^{2} \rangle \langle \mid S_{HV} \mid^{2} \rangle}}, \tag{4.13}$$

$$\rho_{HH/VV} = \frac{\mid \langle S_{HH} S_{VV}^{*} \rangle \mid}{\sqrt{\langle \mid S_{HH} \mid^{2} \rangle \langle \mid S_{VV} \mid^{2} \rangle}}. \tag{4.14}$$

As a first idea the correlation matrix (normalised polarimetric covariance matrix) in a uniform region (a field) between the different amplitude images was calculated:

	HH	HV	VV
HH	1.0	0.0323	0.588
HV		1.0	0.0144
VV			1.0

The cross-polarised and co-polarised components are indeed uncorrelated as is often hypothesized in literature [24, 25, 26]. However, a significant correlation does exist between the two co-polarised components (HH and VV).

The results of some more calculations of the correlation between polarimetric images are shown below. On a set of L-band polarimetric images, regions of 100 by 100 pixels were selected corresponding to examples of different types of land-use. For easy reference the coordinates of the upper left corner of each region within the original image are also given between brackets:

Type		HH	HV	VV
City	HH	1.0	0.362	0.809
(1160,721)	HV		1.0	0.389
	VV			1.0
Forest	HH	1.0	0.136	0.186
(620,7138)	HV		1.0	0.136
	VV			1.0
Runway	HH	1.0	0.057	0.389
(340,2264)	HV		1.0	0.129
	VV			1.0
Short Grass	HH	1.0	0.0449	0.577
(730,2788)	HV		1.0	0.0448
	VV			1.0
Field	HH	1.0	0.032	0.588
(765,7955)	HV		1.0	0.0144
	VV			1.0

Table 4.4: Correlation coefficients between polarimetric components for various types of land cover

For the test image (L-band), in cities, a significant correlation between HH/HV and VV/HV is found. On the other hand, in forests the correlation between HH/HV, HH/VV and VV/HV seem to be similar and relatively low. The correlation between different polarimetric images depends on the wavelength of the radar as well as on the incidence angle, so extrapolation of the behaviours found above should be made with caution.

4.2.4 Relationship between the Spatial and the Interchannel Correlation

The spatial correlation describes the relationship between neighbouring pixels within an image corresponding to a single channel (one polarisation). The interchannel correlation

describes the relationship between different channels; i.e. in our case different polarisations. We would now like to examine the relationship between pixels in one channel C1 to their neighbours in another channel C2. Therefore we define a "combined" correlation function as:

$$\rho(\Delta x, \Delta y, C1 \rightarrow C2) = \frac{\langle (I(x+\Delta x, y+\Delta y, C2) - \mu_I(C2))(I(x,y,C1) - \mu_I(C1)) \rangle}{\sigma_I(C1)\sigma_I(C2)}, \tag{4.15}$$

where C1 and C2 denote the two channels (e.g. HH and VV).

If the correlation within one image is independent of the correlation between the different images, it is possible to write:

$$\rho(\Delta x, \Delta y, C1 \rightarrow C2) = \rho_{C1}(\Delta x, \Delta y)\rho_{\Delta x=0, \Delta y=0}(C1, C2). \tag{4.16}$$

$\rho_{C1}(\Delta x, \Delta y)$ is the spatial correlation in the first image and $\rho_{\Delta x=0,\Delta y=0}(C1, C2)$ is the interchannel correlation defined in the previous section. In order to verify the validity of eq. 4.16, we have determined the average combined correlation function given in eq. 4.15 between HH and VV for a number of uniform regions. In order to eliminate the effect of texture, the subset of the 15 uniform regions of sect. 4.2.1 that were consistent with the average spatial correlation function were used. On the other hand the average spatial correlation function for the same regions was determined in both the HH and the VV component image. The average spatial correlation function (averaged over the two polarisations) was then multiplied with the interchannel correlation coefficient at lag 0,0, according to eq. 4.16. In fig. 4.13 the results are shown. The red solid curve is the spatial correlation within the HH-component image, the blue dashed curve in the spatial correlation within the VV-component image, the green dotted curve is the measured combined correlation corresponding to eq. 4.15, the crosses represent the calculated combined correlation function corresponding to eq. 4.16. Apparently the spatial and interchannel correlations are indeed independent for the regions that were used in this test.

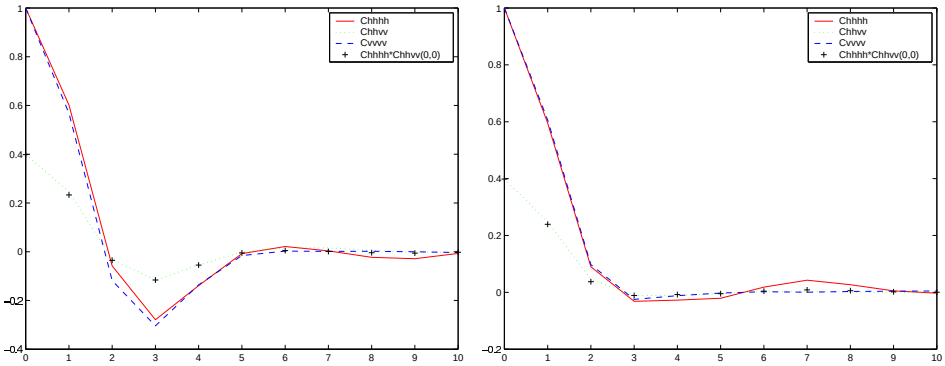

Figure 4.13: Correlation between HH and VV image in range(left) and azimuth (right)

In order to verify the effect of texture, the same experiment was executed for all of the 15 "uniform" regions but this time results were investigated region per region. Two

observations were made:

- contrary to the spatial correlation, the combined correlation function is not necessarily symmetrical

- the maximum of the combined correlation is not always located at lag 0,0

Both effects were only observed in the range direction. In order to investigate these two effect somewhat further, we have plotted the combined correlation and the result of eq. 4.16 for each separate region. This time the maximum of the combined correlation was used in the product instead of the value at lag $0, 0$, i.e. In figs. 4.14 and 4.15 the results are shown. The red dashed curves are the result of eq. 4.15, the blue curves show the result of eq. 4.16. In the title of each subplot the lag corresponding to the maximum of the combined correlation function is shown (format: range, azimuth). In the azimuth all the functions are symmetrical and the maximum is always found at a zero lag. In range this is not the case. An offset of at most one pixel is found in the position of the maximum for some regions and this offset can be either negative or positive. The dissymmetry is the most obvious for region 1. In the figure the constant interchannel correlation used in eq. 4.16 to obtain the blue curve is the maximum of the combined correlation function (and not necessarily the interchannel correlation at lag 0,0).

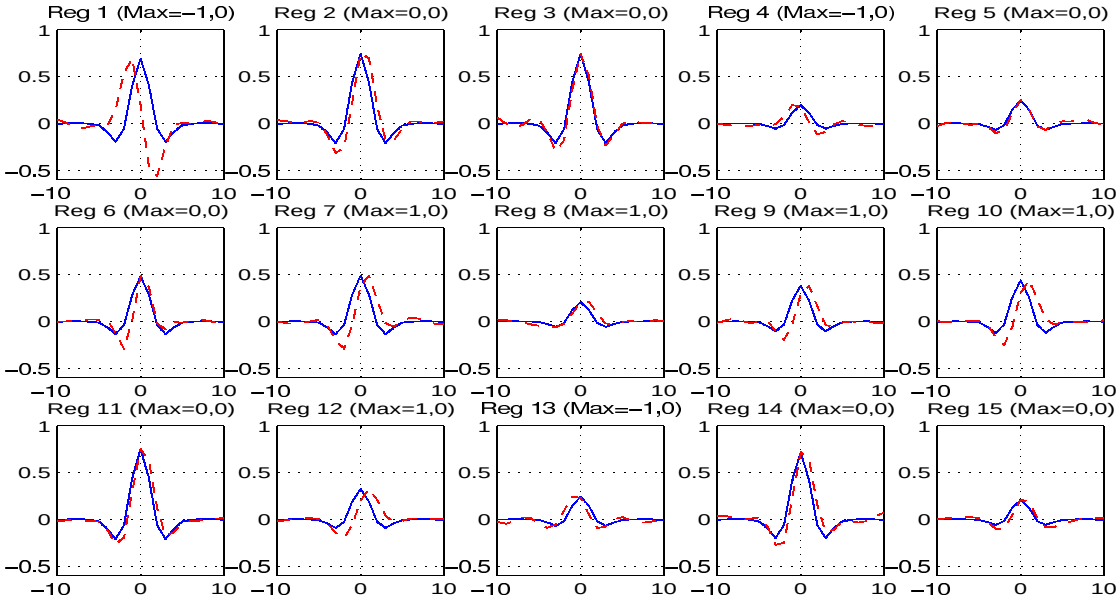

Figure 4.14: Combined correlation function in the range direction for the 15 uniform regions

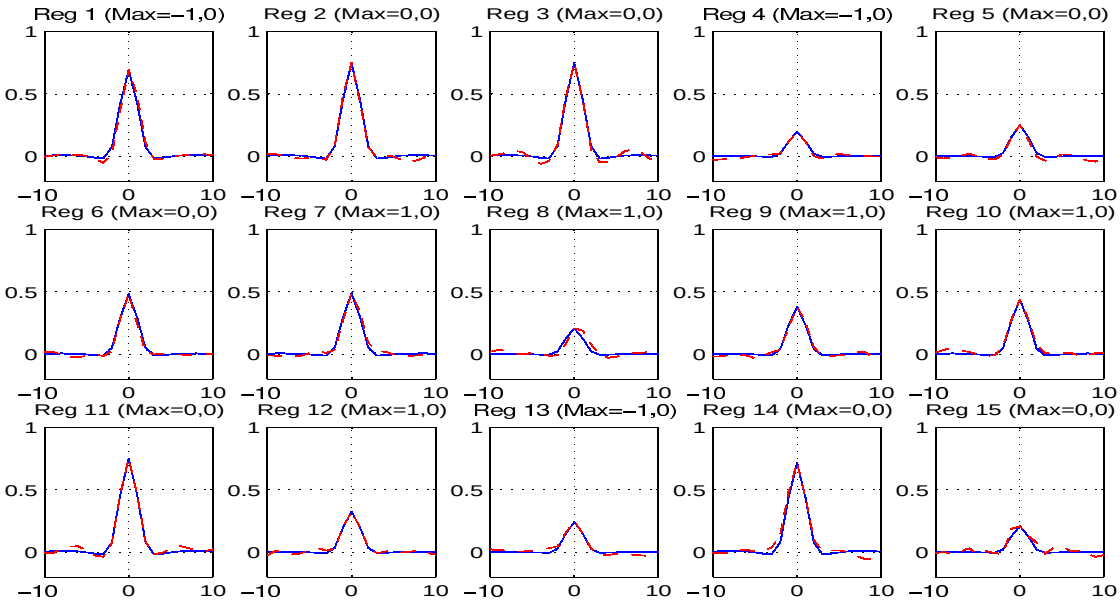

Figure 4.15: Combined correlation function in the azimuth direction for the 15 uniform regions

In order to verify the validity of the independence hypothesis eq. 4.16 in a more formal manner, we applied a hypothesis test for comparison of two correlation coefficients, based on the Fisher transformation of the correlation coefficient. The test was applied for several lags in range and azimuth direction to compare the two sides of eq. 4.16, $\rho_{\Delta x=0,\Delta y=0}(C1, C2)$ being considered constant. For the azimuth direction the hypothesis of was verified for all regions (for a 5% significance level). For the range direction, the hypothesis is rejected for regions 1, 2, 8, 11 and 14.

4.3 Lessons Learned

A uniform region on a SAR image looks noisy due to the presence of speckle. This speckle is an interference phenomenon that can be accurately statictically modeled. In single-look images the statistical distribution of the speckle in uniform regions follows different laws depending on the type of SAR image that is considered. The main characteristics are summarised in table 4.5.

Image Type	Distribution	Comments
Complex	Normal	zero mean, variance is proportional to radar backscattering coefficient
Amplitude	Rayleigh	
Intensity	Exponential	mean is equal to standard deviation
Log-Intensity	Fisher-Tippet	changes in radar backscattering shift the distribution

Table 4.5: Overview of speckle distribution characteristics in uniform regions of a single-look SAR image

For each of the developed detectors we will chose the type of image for which the speckle distribution is most compatible with the detector. In particular the complex image and the log-intensity image will be used.

In the SAR image we find a spatial correlation between neighbouring pixels. This is partly due to the SAR processing and partly to texture features in the terrain. The spatial correlation due to the SAR processing can be related to the impulse response of the system. We will see that the behaviour of the various detection algorithms is influenced by the spatial correlation.

Because we are dealing with polarimetric images, we also investigated the correlation between the three polarisations (the interchannel correlation) as well as the relation between spatial and interchannel correlation. The interchannel correlation between copolar and crosspolar (e.g. HH and HV) component images is zero in most vegetated areas. This is not true in areas with deterministic scatterers (e.g. villages) or when some preferred scattering orientation is present in the scene. This fact will be used in the detection of built-up areas (chapter 7).

The spatial and interchannel correlation were found to be independent in most test regions.